

# Concentration-Driven Assembly and Sol–Gel Transition of $\pi$ -Conjugated Oligopeptides

Yuecheng Zhou,<sup>†</sup> Bo Li,<sup>‡</sup> Songsong Li,<sup>†</sup> Herdeline Ann M. Ardoña,<sup>#ID</sup> William L. Wilson,<sup>§,||</sup> John D. Tovar,<sup>#,¶ID</sup> and Charles M. Schroeder<sup>\*§,‡,†ID</sup>

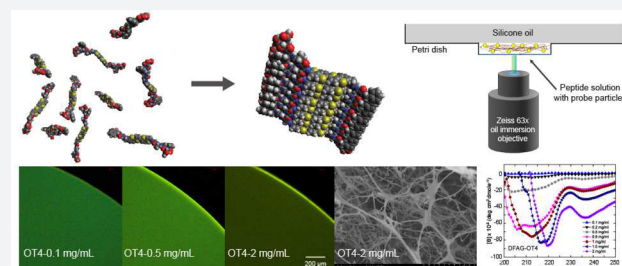
<sup>†</sup>Department of Materials Science and Engineering, <sup>‡</sup>Department of Chemical and Biomolecular Engineering, and <sup>§</sup>Frederick Seitz Materials Research Laboratory, University of Illinois at Urbana-Champaign, Urbana, Illinois 61801, United States

<sup>#</sup>Department of Chemistry and <sup>¶</sup>Department of Materials Science and Engineering, Johns Hopkins University, Baltimore, Maryland 21218, United States

<sup>||</sup>Center for Nanoscale Systems, Faculty of Arts and Sciences, Harvard University, Cambridge, Massachusetts 02138, United States

## Supporting Information

**ABSTRACT:** Advances in supramolecular assembly have enabled the design and synthesis of functional materials with well-defined structures across multiple length scales. Biopolymer-synthetic hybrid materials can assemble into supramolecular structures with a broad range of structural and functional diversity through precisely controlled noncovalent interactions between subunits. Despite recent progress, there is a need to understand the mechanisms underlying the assembly of biohybrid/synthetic molecular building blocks, which ultimately control the emergent properties of hierarchical assemblies. In this work, we study the concentration-driven self-assembly and gelation of  $\pi$ -conjugated synthetic oligopeptides containing different  $\pi$ -conjugated cores (quaterthiophene and perylene diimide) using a combination of particle tracking microrheology, confocal fluorescence microscopy, optical spectroscopy, and electron microscopy. Our results show that  $\pi$ -conjugated oligopeptides self-assemble into  $\beta$ -sheet-rich fiber-like structures at neutral pH, even in the absence of electrostatic screening of charged residues. A critical fiber formation concentration  $c_{\text{fiber}}$  and a critical gel concentration  $c_{\text{gel}}$  are determined for fiber-forming  $\pi$ -conjugated oligopeptides, and the linear viscoelastic moduli (storage modulus  $G'$  and loss modulus  $G''$ ) are determined across a wide range of peptide concentrations. These results suggest that the underlying chemical structure of the synthetic  $\pi$ -conjugated cores greatly influences the self-assembly process, such that oligopeptides appended to  $\pi$ -conjugated cores with greater torsional flexibility tend to form more robust fibers upon increasing peptide concentration compared to oligopeptides with sterically constrained cores. Overall, our work focuses on the molecular assembly of  $\pi$ -conjugated oligopeptides driven by concentration, which is controlled by a combination of enthalpic and entropic interactions between oligopeptide subunits.



## INTRODUCTION

Recent advances in supramolecular chemistry have enabled the design and fabrication of next-generation functional materials.<sup>1,2</sup> Using a bottom-up approach, small molecule building blocks can be directed to self-assemble into organized one-dimensional (1D),<sup>3</sup> two-dimensional (2D),<sup>4</sup> and three-dimensional (3D) structures<sup>5</sup> via noncovalent interactions.<sup>6</sup> The emergent supramolecular architectures exhibit unique mechanical,<sup>7</sup> biological,<sup>8</sup> and electronic properties,<sup>9</sup> all of which can be harnessed to develop tailored functional materials. Specific intermolecular interactions within organic subunits generally govern the nanoscale self-assembly process,<sup>10</sup> such that intricate molecular mechanisms work in concert to guide the formation of complex higher-order structures.<sup>11</sup>

Nature has mastered the ability to order small molecule building blocks into hierarchical assembled structures. Bio-derived building blocks such as amino acids or peptides form diverse heterostructures such as proteins or nucleic acid-

protein structures, which serve to maintain fundamental life processes. Peptides are a versatile subunit that possess high structural controllability and biocompatibility, and self-assembled oligopeptide sequences form stable helical or sheet structures due to stable intermolecular hydrogen bonding (H-bonding). From this perspective, there is a critical need to understand and harness the molecular mechanisms underlying self-assembly, which can be leveraged to enable the continued design and development of functional materials.<sup>12</sup>

Self-assembled 1D structures such as nanowires or nanofibers based on synthetic materials exhibit enhanced anisotropic physical or electronic properties in a single dimension.<sup>13</sup> For example, by carefully programming  $\pi$ -conjugated aromatic units into the organic building blocks, self-assembled 1D structures show the ability to transport charge carriers over long distances

Received: June 19, 2017

Published: August 17, 2017

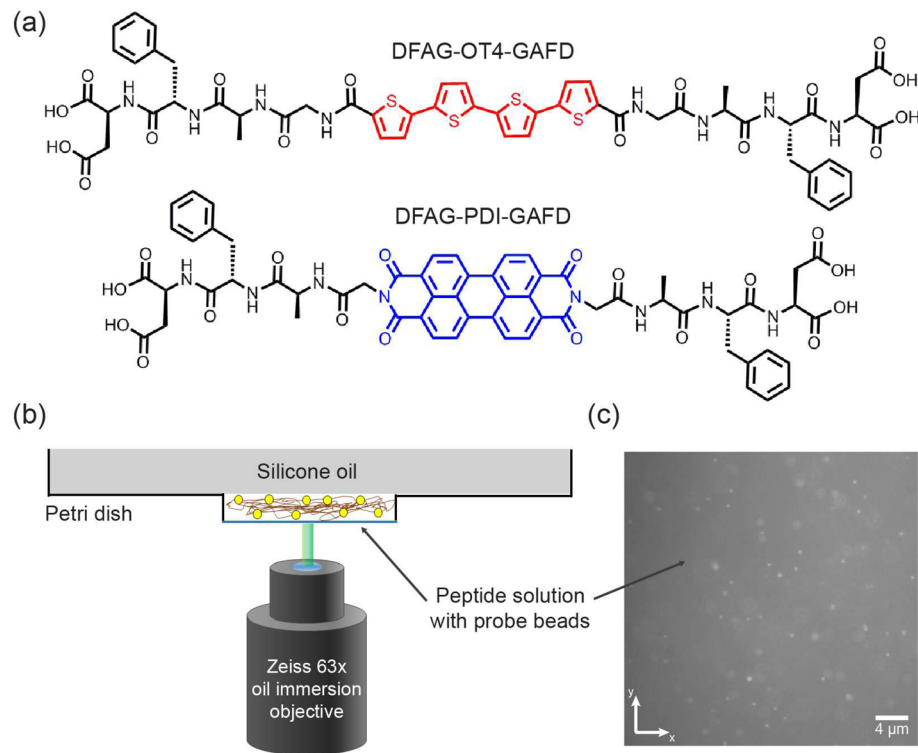


**Figure 1.** Investigating the self-assembly of  $\pi$ -conjugated oligopeptides at neutral pH. (a) Chemical structures of DFAG-OT4 and DFAG-PDI. (b) Schematic of the experimental setup for multiple particle tracking microrheology (PTM). (c) Characteristic image of tracer particles (diameter  $d = 0.84 \mu\text{m}$ ) diffusing in a peptide matrix from fluorescence microscopy.

under pulse-radiolysis.<sup>14</sup> These materials hold the potential to serve as candidate materials for advanced soft semiconducting optoelectronic devices.<sup>15</sup> To this end, aromatic units with electron/hole transport capabilities can be appended to oligopeptide sequences to form well-defined monodisperse subunits with H-bonding motifs.<sup>16,17</sup> Peptide- $\pi$ -conjugated hybrid systems could potentially outperform conventional synthetic  $\pi$ -conjugated systems in terms of structural diversity, sequence controllability, and functional tunability. In particular, synthetic oligopeptides with  $\pi$ -conjugated cores generally show excellent processability in aqueous solutions and were shown to demonstrate hole transport capabilities, thereby providing promising candidate materials for field-effect transistors.<sup>18</sup>

Although the kinetics of self-assembly is known to affect the emergent properties of  $\pi$ -conjugated oligopeptides,<sup>19,20</sup> the molecular mechanisms underlying assembly are not yet fully understood. Previous work has shown that  $\pi$ -conjugated oligopeptides self-assemble into fiber-like structures in acidic conditions due to the formation of H-bonding interactions between peptide flanking sequences.<sup>16,21</sup> For peptides rich in acidic residues (e.g., aspartic acid, glutamic acid), enthalpic H-bonding driving forces dominate the assembly process in acidic conditions due to electrostatic screening effects.<sup>16</sup> From this view, acid-driven assembly has been used as the primary method to induce self-assembly for this class of materials in prior work.<sup>16,19–21</sup> Under kinetically dominated (or reaction-controlled) conditions, acid-driven assembly generally results in rapid molecular assembly, completing within seconds and occurring across an extremely narrow pH window.<sup>19</sup> Under these conditions, it can be challenging to experimentally assess the role of additional enthalpic driving forces such as  $\pi$ - $\pi$  stacking interactions and entropic driving forces such as hydrophobic effects, both of which are known to contribute

to the self-assembly process.<sup>16</sup> Moreover, the vast majority of prior work has focused on investigating material properties after self-assembly process has completed, which generally occurs long after the critical sol–gel transition. Hence, in order to fully understand how molecular-scale interactions govern the overall self-assembly process, we aim to study the mechanical and optical properties of these materials through the sol–gel transition using a mild triggering scheme based on peptide concentration with a tunable parameter window.

In this work, we demonstrate and study the concentration-driven assembly of synthetic oligopeptides containing two different  $\pi$ -conjugated cores (quaterthiophene and perylene diimide). Using a combination of structural and optical tools including particle tracking microrheology (PTM),<sup>22</sup> confocal fluorescence microscopy, circular dichroism (CD), and cryo-electron microscopy, we monitor the self-assembly process *in situ* for  $\pi$ -conjugated oligopeptides under near-equilibrium conditions, without the need for triggering assembly by addition of acid. Our results show that  $\pi$ -conjugated oligopeptides assemble into fiber-like structures upon increasing oligopeptide concentration under aqueous, pH-neutral conditions, even in the absence of electrostatic screening of charged amino acid residues. Microrheology and optical spectroscopy reveal a critical fiber formation concentration ( $c_{\text{fiber}} = 0.1 \text{ mg/mL}$ ) and a critical gel concentration ( $c_{\text{gel}} = 1 \text{ mg/mL}$ ) for quaterthiophene peptides, as well as a critical diffusive exponent  $\alpha_{\text{crit}} = 0.78 \pm 0.04$  for the onset of gelation. Using PTM, the linear viscoelastic moduli of the assembled structures are determined across a wide range of peptide concentrations, which clearly elucidates the sol–gel transition for these materials. Moreover, we find that the molecular structure of the  $\pi$ -conjugated core greatly affects the self-assembly process. Interestingly, oligopeptides containing

oligothiophene cores are observed to assemble into large, micron-scale fibers with  $\beta$ -sheet-rich morphologies upon increasing peptide concentration. On the other hand, oligopeptides containing bulky perylene diimide cores with steric constraints are generally inhibited for assembling into large fibers at neutral pH. Taken together, the combined characterization approach presented in this paper proves to be a powerful method in detecting and monitoring the self-assembly process, and our results could be useful in guiding the design and development of synthetic  $\pi$ -conjugated oligopeptides for future applications in optoelectronic materials.

## RESULTS AND DISCUSSION

**Microrheology of Peptide Solutions: MSDs and Critical Exponent.** We studied the self-assembly of two different sequence-defined synthetic oligopeptides with  $\pi$ -conjugated cores (Figure 1). In particular, synthetic oligopeptides were designed to contain either a quaterthiophene (OT4) core or a perylene diimide (PDI) core situated between symmetric flanking oligopeptides with a primary amino acid sequence Asp-Phe-Ala-Gly (Supporting Information, Figures S1–S3). The overall sequence of the  $\pi$ -conjugated oligopeptides is HO-DFAG-OT4-GAFD-OH (abbreviated as DFAG-OT4) and HO-DFAG-PDI-GAFD-OH (abbreviated as DFAG-PDI), as shown in Figure 1a.

We began by using multiple PTM to study the sol–gel transition of oligopeptide solutions at neutral pH (Figure 1b,c). Using this approach, trace amounts of small fluorescent probe particles are suspended in aqueous solutions of oligopeptide, and the diffusive motion of multiple probe particles is tracked over time. Aqueous solutions of oligopeptide are added to shallow wells in a glass dish mounted on an inverted fluorescence microscope, and a layer of silicone oil is slowly added on top of the aqueous peptide droplet as a barrier to prevent evaporation (Figure 1b). A characteristic image of fluorescent probe particles suspended in an oligopeptide solution is shown in Figure 1c.

Using PTM, the ensemble-averaged mean-squared displacement (MSD) of particles  $\langle \Delta r^2(\tau) \rangle$  is determined as

$$\langle \Delta r^2(\tau) \rangle \equiv \langle (r(\tau) - r(0))^2 \rangle = 4D\tau^{\alpha(\tau)} \quad (1)$$

where  $\langle \cdot \rangle$  represents the ensemble average over many particle trajectories,  $\tau$  is the lag time,  $D$  is the probe particle diffusivity, and  $\alpha(\tau)$  is the diffusive exponent. The power-law diffusive exponent  $\alpha(\tau)$  is calculated as

$$\alpha(\tau) = \frac{d \ln \langle \Delta r^2(\tau) \rangle}{d \ln \tau} \quad (2)$$

In this work, we focus on the long-time limit of the diffusion exponent, such that the diffusive exponent  $\alpha(\tau) = \alpha$  is constant. In Newtonian fluids,  $\alpha = 1.0$ , and probe particles follow Fickian diffusion. For non-Newtonian viscoelastic fluids, it is generally found that probe particles exhibit subdiffusive behavior such that  $0 < \alpha < 1$ .

Mean-squared displacements (MSDs) of probe particles in DFAG-OT4 solutions across a wide range of peptide concentration  $c$  are shown in Figure 2a. At low peptide concentrations (0.025 mg/mL to 0.1 mg/mL), probe particles exhibit Fickian diffusion with diffusive exponent  $\alpha = 1$  characteristic of a simple Newtonian solution, which suggests that isolated peptides or small aggregates are suspended in an aqueous solvent at fairly low concentrations. Interestingly, as

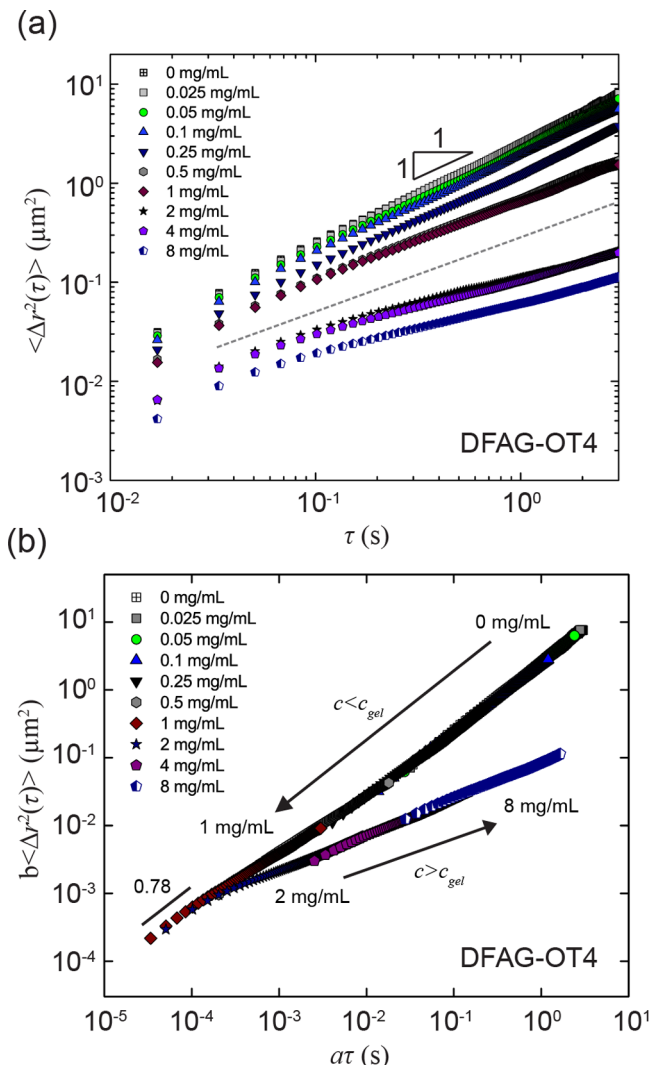


**Figure 2.** Microrheology of the sol–gel transition for DFAG-OT4. (a) Ensemble-averaged MSDs  $\langle \Delta r^2(\tau) \rangle$  versus lag time  $\tau$  for probe particles in DFAG-OT4 solutions at different peptide concentrations. The dashed line shows the slope for the critical diffusive exponent  $\alpha_{\text{crit}} = 0.78$ . (b) Time-cure superposition (TCS) of the MSD for DFAG-OT4 as a function of oligopeptide concentration. The master curve converges with a critical exponent  $\alpha_{\text{crit}} = 0.78 \pm 0.04$  at the critical gel concentration  $c_{\text{gel}} = 1$  mg/mL.

the peptide concentration increases above 0.1 mg/mL,  $\alpha$  begins to deviate from a value of unity, such that subdiffusive behavior is observed to occur for peptide concentrations above 0.1 mg/mL. The onset of this behavior is thought to occur due to changes in local microstructure, such that probe particle thermal motion becomes hindered by the nascent fibers in solution. However, a modest change in  $\alpha$  away from unity suggests that the assembled structures have not yet formed a network in the peptide sample. These data, combined with confocal imaging and electron microscopy data discussed below, suggest that oligopeptides begin to assemble into fibers around a critical fiber concentration  $c_{\text{fiber}} = 0.1$  mg/mL for DFAG-OT4.

The diffusive exponent  $\alpha$  for DFAG-OT4 drops dramatically when peptide  $c$  exceeds 1 mg/mL, which is suggestive of the onset of gelation. In order to probe the sol–gel transition, we performed a time-cure superposition (TCS) analysis to determine the critical exponent  $\alpha_{\text{crit}}$  for DFAG-OT4. By

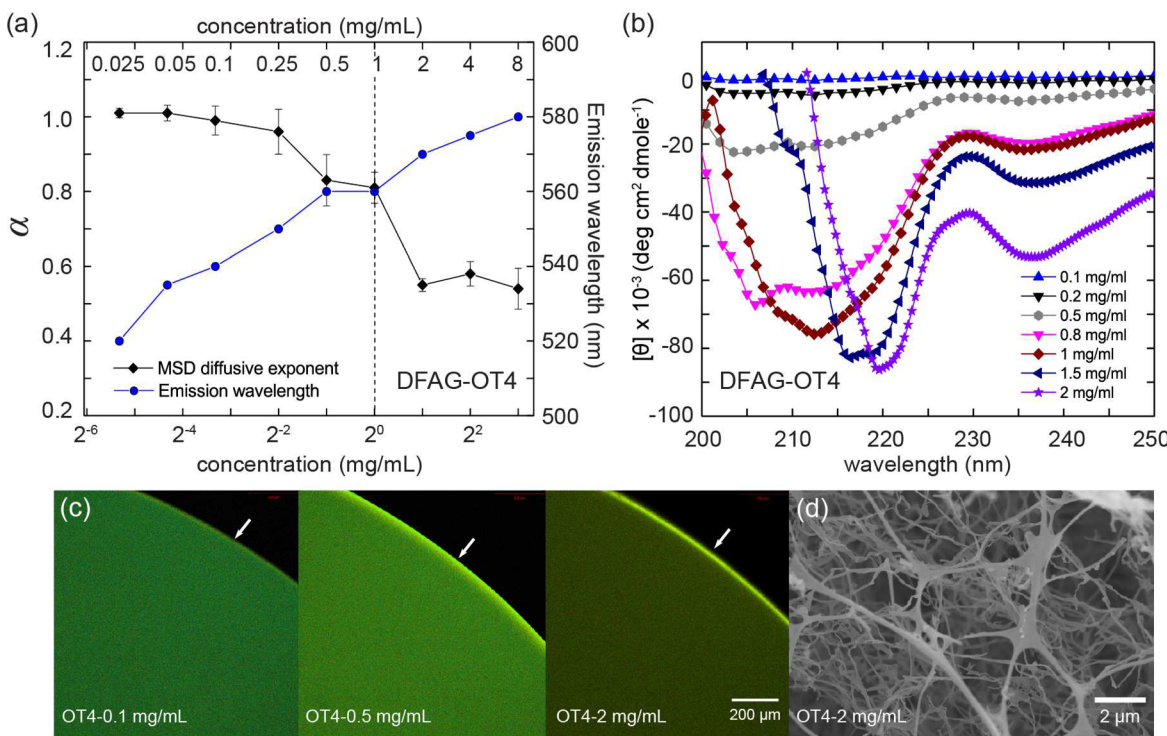


**Figure 3.** Assembly of DFAG-OT4 using a combination of microrheology, optical spectroscopy, and cryo-electron microscopy. (a) Diffusive exponent  $\alpha$  from MSDs and peak fluorescence emission wavelength as functions of peptide concentration for DFAG-OT4. Error bars for the diffusive exponent denote the standard deviation from multiple measurements. (b) CD spectra of DFAG-OT4 as a function of peptide concentration. (c) Confocal fluorescence microscopy images of DFAG-OT4 droplets at different peptide concentrations. Arrows indicate the edge of the droplet. (d) Cryo-SEM image of freeze-dried DFAG-OT4 solution at 2 mg/mL.

shifting the lag time  $\tau$  and the MSD ( $\langle \Delta r^2(\tau) \rangle$ ) by numerical factors of  $a$  and  $b$ , respectively, a master curve is obtained as shown in Figure 2b. The shift factor  $a$  corresponds to a characteristic relaxation time, whereas the factor  $b$  is related to the creep compliance of the system.<sup>23</sup> In this way, TCS can be used to determine the relative amounts of energy stored and dissipated in a material by superposing the viscoelastic response at different stages of assembly as a function of concentration.<sup>23–25</sup> The master curve converges with a terminal of logarithmic slope  $\alpha_{\text{crit}} = 0.78 \pm 0.04$ , which is defined as the critical exponent at the gel point. For diffusive exponents  $\alpha > \alpha_{\text{crit}}$ ,  $\pi$ -conjugated oligopeptides are in a sol phase, wherein small fibers are suspended in a viscous solvent without forming a network. For diffusive exponents  $\alpha < \alpha_{\text{crit}}$ , peptides are in a gel phase, wherein self-assembled fiber structures form a percolated network spanning the entire system.

**Structural and Photophysical Properties of Assembled Structures.** To further probe the molecular properties of  $\pi$ -conjugated oligopeptides during assembly, we studied the concentration-dependent assembly of DFAG-OT4 at neutral pH by combining PTM, confocal fluorescence microscopy, CD, and electron microscopy (Figure 3). As discussed above, microrheology experiments show that the diffusive exponent  $\alpha$  begins to decrease below a value of 1.0 for  $c > c_{\text{fiber}} = 0.1 \text{ mg/mL}$ , and  $\alpha$  precipitously decreases below the critical exponent  $\alpha_{\text{crit}} = 0.78$  at a critical gel concentration  $c_{\text{gel}} = 1 \text{ mg/mL}$  (Figure 3a). For peptide concentrations  $c > c_{\text{gel}}$ , the diffusive exponent  $\alpha \approx 0.5$ , which suggests that the assembled DFAG-OT4 material is comprised of a percolated gel network. Prior studies have determined critical gel exponents  $\alpha_{\text{crit}}$  ranging between 0.5 and 0.8 for fractal-like polymer growth, which is the mechanism expected for the assembly of fiber-

forming peptide networks.<sup>25</sup> We further probed the fluorescence emission spectra to track the progression of  $\pi-\pi$  stacking interactions in the  $\pi$ -conjugated cores at different stages of assembly. Interestingly, the peak fluorescence emission wavelength exhibits a bathochromic shift upon increasing peptide concentration (Figure 3a). The red-shifted fluorescence emission is further evident in confocal fluorescence microscopy images of aqueous droplets of DFAG-OT4, especially at the edge of the droplets (Figure 3c). The red shift in fluorescence emission wavelength suggests a face-to-face molecular ordering of OT4 cores that can be associated with classic H-aggregation.<sup>12,26</sup> Indeed, for  $c > c_{\text{gel}}$ , the fluorescence emission wavelength red-shifts more than 60 nm.

To further probe the molecular-scale ordering of DFAG-OT4 during assembly, we performed CD measurements of DFAG-OT4 as a function of increasing peptide concentration at neutral pH (Figure 3b). In general, CD data show evidence of increased molecular ordering upon increasing peptide concentration, which is consistent with a decreasing diffusive exponent  $\alpha$  (suggesting an approach toward a gel phase) and red-shifted emission wavelength (suggesting  $\pi-\pi$  stacking interactions between  $\pi$ -conjugated cores). For peptide concentrations  $c > c_{\text{fiber}}$ , CD absorption spectra show a broad minimum that shifts toward 218 nm, which is characteristic of  $\beta$ -sheet formation.<sup>27</sup> Interestingly, CD data show that peptide subunits self-assemble toward a  $\beta$ -sheet-rich structure for peptide concentrations  $c_{\text{fiber}} < c < c_{\text{gel}}$ , which occurs before the onset of the sol–gel transition at  $c_{\text{gel}}$ . Therefore, CD spectra confirm that oligopeptide interactions gradually give rise to hydrogen-bonded structures upon increasing peptide concentration, likely due to interactions between adjacent peptide flanking sequences, which occurs before the onset of gelation.

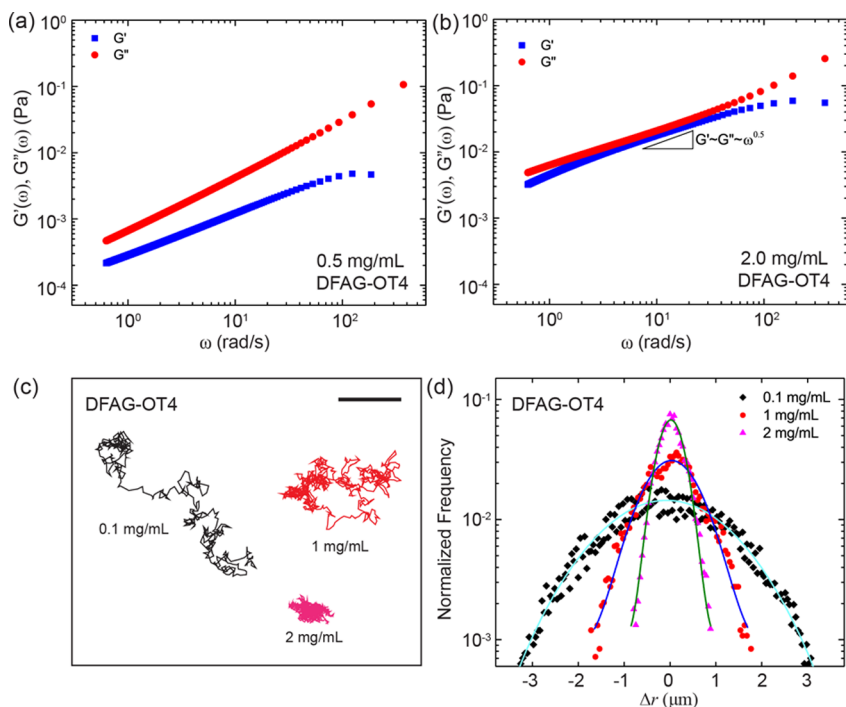


**Figure 4.** Viscoelastic moduli  $G'(\omega)$  and  $G''(\omega)$  as a function of frequency  $\omega$  determined from microrheology experiments for DFAG-OT4 at neutral pH (pH = 7) at (a) 0.5 mg/mL and (b) 2 mg/mL. (c) Representative probe particle trajectories and (d) van Hove correlation functions of probe particle trajectories at peptide concentrations of 0.1 mg/mL, 1 mg/mL, and 2 mg/mL. Solid lines are Gaussian fits. Scale bar = 2  $\mu\text{m}$ .

Finally, we performed cryo-electron microscopy on the assembled DFAG-OT4 materials. Scanning electron microscopy (SEM) images obtained from freeze-dried DFAG-OT4 solutions (2 mg/mL) directly reveal the existence of interlaced 3D percolated networks with an average mesh size  $\lesssim 1 \mu\text{m}$  (Figure 3d).

In addition to studying the concentration-driven self-assembly of oligopeptides at neutral pH, we also studied the pH-driven assembly of DFAG-OT4 under acidic conditions.<sup>19,20</sup> Here, we triggered the self-assembly of DFAG-OT4 by allowing acid vapor to slowly diffuse through a layer of silicone oil that isolates an aqueous droplet of DFAG-OT4 (Figure 1b), as previously described.<sup>19</sup> In these experiments, we also used microrheology to track the sol–gel transition of an aqueous solution of DFAG-OT4 containing probe particles under diffusion-dominated conditions (Figure S4). The formation of assembled fibers in acidic conditions is indicated by a shift in the MSD of probe particle diffusion away from simple Fickian diffusion, such that the diffusive exponent  $\alpha < 1$ . For kinetically controlled acid-driven self-assembly, the onset of gelation occurs at  $t = 10$  h when the diffusive exponent  $\alpha \approx \alpha_{\text{crit}}$  and completes at  $t = 16$  h with a diffusive exponent  $\alpha \approx 0.1$ , which is much smaller than  $\alpha_{\text{crit}}$ . This suggests the gel formed through acid-driven assembly is a strong gel (storage dominated). On the other hand, the gel formed via concentration-driven assembly at  $c > c_{\text{gel}}$  shows a diffusive exponent  $\alpha \approx 0.5$ , which is indicative of a weak gel.

Prior work has shown that DFAG-OT4 peptides self-assemble into fiber-like structures via hydrogen bonding interactions in acidic conditions due to protonation of aspartic acid residues for  $\text{pH} < \text{p}K_a$  for Asp.<sup>16</sup> Under these conditions, electrostatic repulsions are screened and  $\pi$ -conjugated oligopeptides assemble into fiber-like structures via intermolecular H-bonding interactions between peptide flanking

sequences and  $\pi-\pi$  interactions between adjacent  $\pi$ -conjugated cores. The acid-driven self-assembly process leads to a hypsochromic shift in absorption and quenched bathochromic shift in fluorescence emission (Figure S5), which can be attributed to the ordering of  $\pi$ -conjugated cores and is a signature for the formation of H-aggregate stacks within the molecular subunits.<sup>26</sup> Hence, despite differences in micro-mechanics, the molecular structure of the assembled fibers from both acid-driven and concentration driven assembly appears to be similar.

**Concentration-Driven Assembly of  $\pi$ -Conjugated OT4 Oligopeptides.** Taken together, the results in Figures 2 and 3 suggest that DFAG-OT4 oligopeptides assemble into higher-order fiber-like structures without triggering assembly under acidic conditions. Concentration-driven assembly can be understood by considering  $\pi-\pi$  stacking interactions and dispersive interactions within the OT4 cores.<sup>28</sup> Upon increasing concentration, peptide aggregation is mediated by  $\pi-\pi$  stacking of quaterthiophene cores, which further facilitates H-bonding interactions between adjacent peptides in the flanking sequences. Apparently, assembly occurs even under neutral pH conditions (pH = 7.0), where electrostatic repulsions are present due to negative charges on aspartic acid residues. Interestingly,  $\pi$ -stacking interactions of the OT4 cores alone are not sufficient to induce assembly. Under basic conditions (pH = 8 and pH = 14), no evidence of peptide assembly was observed using microrheology, even for peptide concentrations above the fiber formation concentration  $c > c_{\text{fiber}}$  (Figure S6). Under basic solution conditions, strong electrostatic repulsions hinder aggregation of peptides into large assembled structures; however, recent coarse-grained molecular dynamics simulations have shown that some  $\pi$ -conjugated peptides associate into small aggregates under these conditions.<sup>29</sup>

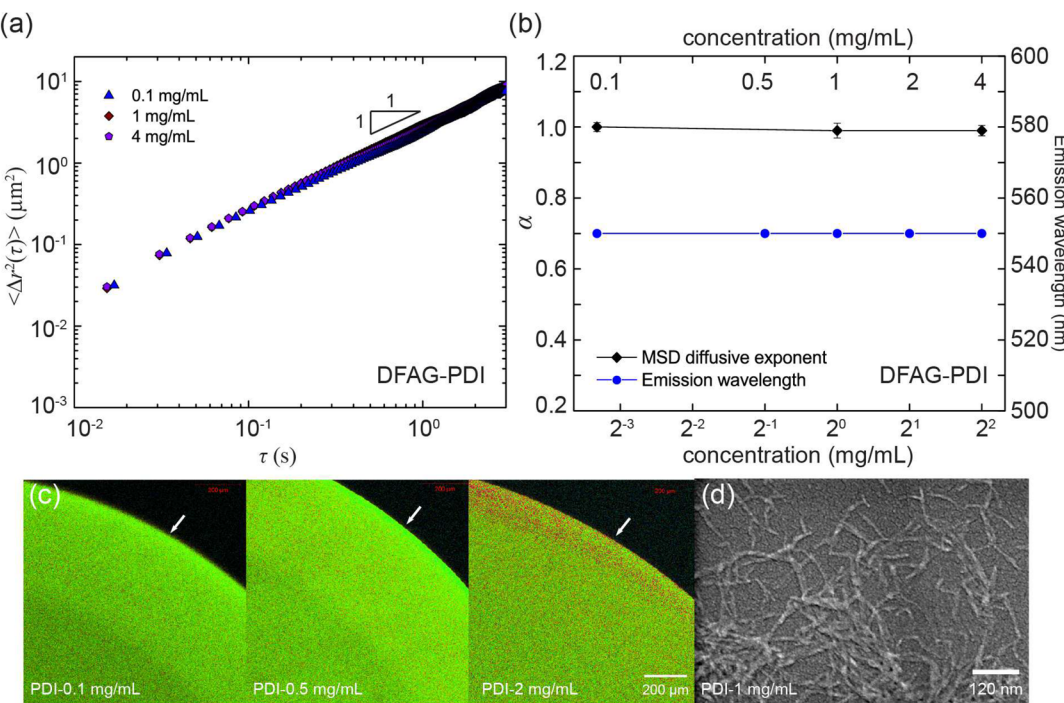


**Figure 5.** Assembly of DFAG-PDI using a combination of microrheology, optical spectroscopy, and cryo-electron microscopy. (a) Ensemble-averaged MSDs ( $\langle \Delta r^2(\tau) \rangle$ ) as a function of lag time  $\tau$  for probe particles in DFAG-PDI solutions with different concentrations. (b) Diffusive exponent  $\alpha$  from microrheology and peak fluorescence emission wavelength as functions of peptide concentration for DFAG-PDI. Error bars for the diffusive exponent denote the standard deviation from multiple measurements. (c) Confocal fluorescence microscopy images of DFAG-PDI droplets at different concentrations. Arrow indicate the edge of the droplet. (d) Cryo-SEM image of DFAG-PDI solution at 1 mg/mL.

Optical spectroscopy, microrheology, and cryo-EM experiments demonstrate that fiber-like structures form in DFAG-OT4 solutions upon increasing peptide concentration. In fact, concentration-dependent self-assembly driven by  $\pi-\pi$  interactions has been observed in synthetic  $\pi$ -conjugated supramolecular systems based on discotic molecules, when the degree of polymerization increases with monomer concentration.<sup>30</sup> For synthetic  $\pi$ -conjugated oligopeptides, however, concentration-dependent assembly is thought to be driven by a combination of enthalpic forces (H-bonding and  $\pi-\pi$  stacking interactions) and entropic forces (hydrophobic effects).<sup>16</sup> On the other hand, the pH-driven sol–gel transition is challenging to observe, mainly due to a narrow window of pH in the vicinity of the transition (Figure S7), combined with a rapid molecular assembly process that usually completes within seconds due to H-bonding interactions between the peptide flanking sequences.<sup>19</sup> From this perspective, using peptide concentration as the external parameter controlling assembly, the sol–gel process can be probed across a wide range of experimentally accessible conditions.

**Linear Viscoelastic Moduli and Structural Homogeneity.** We further determined the linear viscoelastic moduli (storage modulus  $G'(\omega)$  and loss modulus  $G''(\omega)$ ) as a function of frequency  $\omega$  using probe microrheology. The viscoelastic moduli of a sample can be determined from the measurement of  $\langle \Delta r^2(\tau) \rangle$  using the generalized Stokes–Einstein relation (GSER) under the assumption that probe particles are in a continuum and particle inertia is negligible,<sup>31,32</sup> such that

$$G^*(\omega) = \frac{k_b T}{\pi a i \omega \mathcal{F}_u \langle \langle \Delta r^2(\tau) \rangle \rangle} \quad (3)$$

where  $k_b$  is the Boltzmann constant,  $\mathcal{F}_u \langle \langle \Delta r^2(\tau) \rangle \rangle$  is the unilateral complex Fourier transform of the mean-squared displacement,<sup>33</sup>  $i$  is the imaginary unit,  $a$  is probe (bead) radius, and  $G^*(\omega)$  is the complex modulus defined as

$$G^*(\omega) = G'(\omega) + iG''(\omega) \quad (4)$$

For discrete MSD data acquired from the experiment, the complex modulus  $G^*(\omega)$  can be approximated as

$$G^*(\omega) \approx \frac{k_b T \exp[i\pi\alpha(\omega)/2]}{\pi a i \langle \Delta r^2(1/\omega) \rangle \Gamma[1 + \alpha(\omega)]} \quad (5)$$

where  $\Gamma$  is the  $\Gamma$ -function and the angular frequency  $\omega = 1/\tau$ .

The viscoelastic moduli  $G'$  and  $G''$  for DFAG-OT4 are shown in Figure 4a,b under neutral pH conditions ( $\text{pH} = 7$ ) at two different peptide concentrations. For a peptide concentration of 0.5 mg/mL (such that  $c_{\text{fiber}} < c < c_{\text{gel}}$ ), the loss modulus  $G''(\omega)$  dominates the storage modulus  $G'$  at all frequencies, which suggests that the peptide solution is viscous-like and the nascent fibers have not yet formed an entangled network. For a peptide concentration of 2 mg/mL (such that  $c > c_{\text{gel}}$ ), the loss and storage moduli scale with nearly the same power-law relation as a function of frequency, such that  $G'(\omega) \approx G''(\omega) \approx \omega^{1/2}$ . This behavior is a signature of the critical gel point according to the Chambon and Winter criterion.<sup>34,35</sup> Here, the storage modulus  $G' \approx 0.06 \text{ Pa}$ , which is characteristic of a mechanically weak incipient gel. These results are consistent with the data and conclusions drawn from the diffusive exponent, as discussed above.

We further investigated the structural homogeneity of DFAG-OT4 oligopeptide solutions (Figure 4c,d). Representative probe particle trajectories are shown in Figure 4c in DFAG-OT4 solutions at different peptide concentrations. Upon

increasing peptide concentration, probe particle motion becomes increasingly restrained due to the formation of a fiber network. To quantify these data, we determined van Hove correlation functions showing the probability of probe particle displacement  $\Delta r$  for lag times between  $0 \text{ s} < \tau < 1.7 \text{ s}$  over at least 8000 data points, as shown in Figure 4d. Experimental data are fit to a Gaussian function:

$$P(\Delta r, \tau) = \frac{1}{(4\pi D\tau)^{1/2}} \exp\left(\frac{-\langle (\Delta r)^2 \rangle}{4D\tau}\right) \quad (6)$$

where  $P(\Delta r, \tau)$  is the probability of particle displacement as a function of lag time  $\tau$ . Equation 6 is used to fit the data before gelation at  $c < c_{\text{gel}}$  during the sol–gel transition at  $c = c_{\text{gel}}$ , and after gelation at  $c > c_{\text{gel}}$ . The Gaussian function shows good agreement with experimental data, indicating that the system is purely diffusive. Probe particle motion can be described by a simple random walk with decreasing diffusion constant, which is reflected from the reduced variance of the Gaussian distribution. Moreover, Gaussian statistics of a van Hove correlation function serve as a good indicator of sample homogeneity,<sup>36</sup> such that particle displacement  $\Delta r$  for individual probe particles can be described by the same diffusion constant. In this way, we observe no evidence of sample inhomogeneities during the sol–gel transition for  $c > c_{\text{gel}}$  for DFAG-OT4.

**Effect of  $\pi$ -Conjugated Core on Oligopeptide Assembly.** We further sought to study the effect of  $\pi$ -conjugated cores on the self-assembly of synthetic oligopeptides. For these experiments, we again applied the combined experimental approach including microrheology, optical spectroscopy, and cryo-EM to aqueous solutions of DFAG-PDI (Figure 5). Microrheology reveals that the diffusive exponent  $\alpha = 1$  for peptide concentrations ranging between 0.1 and 4 mg/mL at neutral pH (Figure 5a). In all cases, the oligopeptide solution remains Newtonian with the apparent lack of network formation upon increasing peptide concentration. Although DFAG-OT4 and DFAG-PDI oligopeptides share the same amino acid flanking sequences, the diffusive exponent and peak fluorescence emission wavelength remain constant for DFAG-PDI across a wide range of peptide concentrations (Figure 5b), which starkly contrasts the behavior of DFAG-OT4 (Figure 3a). Moreover, confocal fluorescence images of DFAG-PDI droplets show no change in color upon increasing peptide concentration (Figure 5c), which again contrasts DFAG-OT4 (Figure 3c). Interestingly, SEM images of DFAG-PDI reveal the formation of few extremely short fibers on the order of size  $\sim 100 \text{ nm}$  (Figure 5d), which is consistent with apparent Newtonian behavior of the solution and lack of spectral shifts even at high peptide concentrations.

The OT4 core is connected by three C–C bonds (between  $\text{sp}^2$  carbon atoms), thereby resulting in additional degrees of torsional flexibility compared to PDI. Indeed, the bulky PDI core in DFAG-PDI can be viewed as two naphthalene half units connected together by C–C bonds, thereby resulting in a large  $\pi$ -conjugated aromatic core. The steric strain in the two half-units tends to twist the PDI core into a propeller-like structure with an angle of  $\sim 30^\circ$ .<sup>37</sup> The twist in the  $\pi$ -conjugated core is also reflected in the unique vibronic secondary peak in the fluorescence emission spectrum (Figure S8).<sup>38</sup> The distortion of PDI core from planarity restricts the aggregation and packing of the DFAG-PDI monomers, despite the appended peptide flanking sequences that adds some degrees of freedom and the

potential for H-bonding. Therefore, the potential attractive enthalpic interactions are not able to overcome the large degree of steric repulsion originating from the PDI core at neutral pH (pH = 7), which likely precludes the assembly of DFAG-PDI into long fibers and percolated networks upon increasing peptide concentration. Finally, DFAG-PDI can be induced to self-assemble under acidic conditions at low pH (Figures S8 and S9), presumably by screened electrostatic repulsions, as indicated from the hypsochromic shift in the absorption spectrum and quenched bathochromic shift in the fluorescence emission spectrum.

## CONCLUSION

In this work, we combine multiple particle tracking microrheology, confocal fluorescence microscopy, optical spectroscopy, and electron microscopy to investigate the structural and optical properties of  $\pi$ -conjugated oligopeptides across a wide range of peptide conditions. Self-assembly and *in situ* fiber formation is monitored in solution under near-equilibrium conditions using both concentration-driven assembly and acid-driven assembly. Our results show that  $\pi$ -conjugated oligopeptides with relatively flexible OT4 cores self-assemble into fiber-like structures under neutral pH (pH = 7); however, peptides with sterically constrained PDI cores show no evidence of assembly upon increasing peptide concentration at neutral pH. For DFAG-OT4, microrheology and fluorescence emission spectra indicate the existence of a critical fiber concentration  $c_{\text{fiber}} = 0.1 \text{ mg/mL}$  and a critical gel concentration  $c_{\text{gel}} = 1 \text{ mg/mL}$  with a critical diffusive exponent  $\alpha_{\text{crit}} = 0.78 \pm 0.04$  from time-cure superposition (TCS) analysis. CD spectra confirm the formation of  $\beta$ -sheet-rich fiber structures at  $c > c_{\text{gel}}$  for DFAG-OT4, and the loss modulus  $G''(\omega)$  dominates at  $c < c_{\text{gel}}$  while at  $c > c_{\text{gel}}$ ,  $G'(\omega) \approx G''(\omega)$ , which is the hallmark of a critical incipient gel. Moreover, probe particle trajectories are well described by Gaussian statistics, which suggests that the materials remain homogeneous before and after the sol–gel transition. Compared to acid-driven self-assembly, the gel formed through concentration-driven assembly is much weaker, but the molecular stacking structures resulting from both schemes are similar.

The combined microrheology–spectroscopy approach in this work is useful in elucidating the structural and optical properties of  $\pi$ -conjugated oligopeptides. This powerful approach enables effective monitoring and control over the self-assembly process for synthetic  $\pi$ -conjugated oligopeptides *in situ*, which can be challenging to achieve. Given the potential applications for biohybrid synthetic peptides in electronic materials, conductive fibers or gels possessing specified mechanical strengths could be assembled and manufactured in a controlled fashion by precisely tuning concentration and/or acid diffusion time. Furthermore, our results further help to illuminate the fundamental self-assembly mechanisms for synthetic  $\pi$ -conjugated oligopeptides in solution under pH-neutral conditions. Taken together, these results may benefit the solution processing of  $\pi$ -conjugated oligopeptides for next-generation optoelectronic materials, while further informing bottom-up design rules for new classes of molecular building blocks.

## EXPERIMENTAL METHODS

**Materials.** Two different sequence-defined synthetic oligopeptides with  $\pi$ -conjugated cores were synthesized using

solid phase peptide synthesis (SPPS), as previously described.<sup>39,40</sup> Experimental details regarding peptide synthesis and analytical characterization are shown in Supporting Information (Figures S1–S3). Synthetic oligopeptides contained either a quaterthiophene (OT4) core or a perylene diimide (PDI) core situated between symmetric flanking oligopeptides with a primary amino acid sequence Asp-Phe-Ala-Gly. The overall sequence of the  $\pi$ -conjugated oligopeptides is HO-DFAG-OT4-GAFD-OH (abbreviated as DFAG-OT4) and HO-DFAG-PDI-GAFD-OH (abbreviated as DFAG-PDI).

**Multiple Particle Tracking Microrheology.** DFAG-OT4 and DFAG-PDI peptides were dissolved in distilled, deionized water (Millipore, conductivity 18 M $\Omega$ ·cm). An aqueous solution of peptide (50  $\mu$ L) containing 2 v/v% fluorescent polystyrene tracer particles (diameter  $d = 0.84 \mu\text{m}$ , Spherotech) is added to the center of a Petri dish with cover glass bottom (FluoroDish). A layer of silicone oil (dynamic viscosity  $\eta = 1000 \text{ cP}$  at  $T = 22.5^\circ\text{C}$ , Sigma-Aldrich) is slowly added on top of the aqueous peptide droplet as a barrier to prevent evaporation. Imaging is performed using an inverted fluorescence microscope (IX71, Olympus) coupled to a standard charge-coupled device (CCD) camera (Grasshopper3, Point Gray). Samples are illuminated using a 100 W mercury arc lamp (USH102D, UShio) directed through a 12% neutral density filter (Olympus), a 535 nm band-pass excitation filter (HQ535/30m, Chroma), and a 550 nm single-edge dichroic mirror (Chroma). Fluorescence emission is collected by a 1.4 NA 63 $\times$  oil immersion objective lens (UPlanSApo, Zeiss), and a 585 nm emission filter (D585/30m, Chroma) is used in the detection path. For each experiment, the motion of at least 100 in-frame particles is acquired using a CCD camera (1024  $\times$  1024 pixels, 5.86  $\mu\text{m}$  pixel size) for  $\sim$ 1000 frames at a frame rate of 59 Hz for enhanced short-time resolution. All experiments are conducted at  $T = 22.5^\circ\text{C}$ . The center-of-mass positions of tracer particles are determined using a custom Matlab program, and particle positions in consecutive video frames are linked to form trajectories.<sup>41,42</sup> Static errors during microrheology experiments are determined by tracking the MSD of probe particles arrested in 3% w/w agarose gel, which is used to correct particle trajectories.<sup>43,44</sup> Assembled peptide structures are not affected by the addition of probe particles, which suggests that the particles generally exhibit minimal nonspecific interactions with the peptides in solution.<sup>45</sup>

**Structural and Optical Characterization.** Cryo-electron microscopy (cryo-EM) was used for structural characterization of assembled peptides. In these experiments,  $\pi$ -conjugated oligopeptide samples are rapidly frozen using liquid nitrogen, dried under a vacuum to maximally retain sample morphology in solution, and imaged using a Hitachi S4800 high-resolution scanning electron microscope (SEM). Confocal fluorescence microscopy was also used for optical and structural characterization of microstructure. In these experiments, a multiphoton confocal microscope (Zeiss 710) was used to determine the fluorescence emission spectra of both unassembled and assembled DFAG-OT4 and DFAG-PDI. Here, DFAG-OT4 samples were illuminated using two-photon excitation at a wavelength of 780 nm using a Ti-Sapphire laser (Mai-Tai, Spectraphysics), and DFAG-PDI samples were illuminated using one-photon excitation at a wavelength of 405 nm. UV-vis absorption spectra were determined using a Cary 5000 UV-vis spectrometer (Agilent). CD spectra were obtained using a JASCO J-815 CD spectrometer.

## ASSOCIATED CONTENT

### S Supporting Information

The Supporting Information is available free of charge on the ACS Publications website at DOI: [10.1021/acscentsci.7b00260](https://doi.org/10.1021/acscentsci.7b00260).

General solid phase peptide synthesis (SPPS) methods for DFAG-OT4 and DFAG-PDI peptides; analytical HPLC traces for DFAG-PDI peptides; electrospray ionization mass spectrometry spectra of pure DFAG-PDI peptides; NMR spectra of purified DFAG-PDI peptides; methods and particle tracking microrheology for acid-vapor-induced assembly of DFAG-OT4 peptide; particle tracking microrheology for DFAG-OT4 peptide under basic (low pH) conditions; absorption and fluorescence emission spectra for unassembled and assembled DFAG-OT4 and DFAG-PDI peptides through acid-vapor-induced assembly and concentration-driven assembly ([PDF](#))

## AUTHOR INFORMATION

### Corresponding Author

\*E-mail: [cms@illinois.edu](mailto:cms@illinois.edu).

### ORCID

Herdeline Ann M. Ardoña: [0000-0003-0640-1262](#)

John D. Tovar: [0000-0002-9650-2210](#)

Charles M. Schroeder: [0000-0001-6023-2274](#)

### Notes

The authors declare no competing financial interest.

## ACKNOWLEDGMENTS

The authors acknowledge the Frederick Seitz Materials Research Laboratory for facilities and instrumentation, and we thank Andrew Ferguson for useful discussions. This work was supported by the U.S. Department of Energy, Office of Science, Basic Energy Sciences Research (BES) under Award No. SC-0011847. H.A.M.A. acknowledges a graduate fellowship through the Howard Hughes Medical Institute (International Student Research Fellowship) and the Schlumberger Foundation (Faculty for the Future Fellowship).

## REFERENCES

- (1) Lehn, J.-M. Toward Self-Organization and Complex Matter. *Science (Washington, DC, U. S.)* **2002**, *295*, 2400–2403.
- (2) Aida, T.; Meijer, E. W.; Stupp, S. I. Functional Supramolecular Polymers. *Science* **2012**, *335*, 813–817.
- (3) Hartgerink, J. D.; Beniash, E.; Stupp, S. I. Self-Assembly and Mineralization of Peptide-Amphiphile Nanofibers. *Science (Washington, DC, U. S.)* **2001**, *294*, 1684–1688.
- (4) Stupp, S. I. Supramolecular Materials: Self-Organized Nanostructures. *Science (Washington, DC, U. S.)* **1997**, *276*, 384–389.
- (5) Wang, Q.; Mynar, J. L.; Yoshida, M.; Lee, E.; Lee, M.; Okuro, K.; Kinbara, K.; Aida, T. High-water-content mouldable hydrogels by mixing clay and a dendritic molecular binder. *Nature* **2010**, *463*, 339–343.
- (6) Hoeben, F. J. M.; Jonkheijm, P.; Meijer, E. W.; Schenning, A. P. H. J. About Supramolecular Assemblies of  $\pi$ -Conjugated Systems. *Chem. Rev.* **2005**, *105*, 1491.
- (7) Sijbesma, R. P.; et al. Reversible polymers formed from self-complementary monomers using quadruple hydrogen bonding. *Science (Washington, DC, U. S.)* **1997**, *278*, 1601–1604.
- (8) Zhang, S. Fabrication of novel biomaterials through molecular self-assembly. *Nat. Biotechnol.* **2003**, *21*, 1171–1178.
- (9) Schmidt-Mende, L.; Fechtenköetter, A.; Müllen, K.; Moons, E.; Friend, R. H.; MacKenzie, J. D. Self-organized discotic liquid crystals

- for high-efficiency organic photovoltaics. *Science (Washington, DC, U. S.)* **2001**, *293*, 1119–1122.
- (10) Ikkala, O.; et al. Functional materials based on self-assembly of polymeric supramolecules. *Science (Washington, DC, U. S.)* **2002**, *295*, 2407–2409.
- (11) Hill, J. P.; Jin, W.; Kosaka, A.; Fukushima, T.; Ichihara, H.; Shimomura, T.; Ito, K.; Hashizume, T.; Ishii, N.; Aida, T. Self-Assembled Hexa-peri-hexabenzocoronene Graphitic Nanotube. *Science* **2004**, *304*, 1481–1483.
- (12) Marciel, A. B.; Tanyeri, M.; Wall, B. D.; Tovar, J. D.; Schroeder, C. M.; Wilson, W. L. Fluidic-directed assembly of aligned oligopeptides with  $\pi$ -conjugated cores. *Adv. Mater.* **2013**, *25*, 6398–6404.
- (13) Palmer, L. C.; Stupp, S. I. Molecular Self-Assembly into One-Dimensional Nanostructures. *Acc. Chem. Res.* **2008**, *41*, 1674–1684.
- (14) Schenning, A. P. H. J.; Meijer, E. W. Supramolecular electronics; nanowires from self-assembled  $\pi$ -conjugated systems. *Chem. Commun.* **2005**, *3245*.
- (15) Xiao, S.; Tang, J.; Beetz, T.; Guo, X.; Tremblay, N.; Siegrist, T.; Zhu, Y.; Steigerwald, M.; Nuckolls, C. Transferring self-assembled, nanoscale cables into electrical devices. *J. Am. Chem. Soc.* **2006**, *128*, 10700–10701.
- (16) Tovar, J. D. Supramolecular construction of optoelectronic biomaterials. *Acc. Chem. Res.* **2013**, *46*, 1527–1537.
- (17) Wall, B. D.; Zhou, Y.; Mei, S.; Ardoña, H. A. M.; Ferguson, A. L.; Tovar, J. D. Variation of formal hydrogen-bonding networks within electronically delocalized  $\pi$ -conjugated oligopeptide nanostructures. *Langmuir* **2014**, *30*, 11375–11385.
- (18) Besar, K.; Ardon, H. A.; Tovar, J. D.; Katz, H. E. Demonstration of Hole Transport and Voltage Equilibration in Self-Assembled  $\pi$ -Conjugated Peptide. *ACS Nano* **2015**, *9*, 12401–12409.
- (19) Li, B.; Li, S.; Zhou, Y.; Ardoña, H. A. M.; Valverde, L. R.; Wilson, W. L.; Tovar, J. D.; Schroeder, C. M. Nonequilibrium Self-Assembly of  $\pi$ -Conjugated Oligopeptides in Solution. *ACS Appl. Mater. Interfaces* **2017**, *9*, 3977–3984.
- (20) Ardoña, H. A. M.; Draper, E. R.; Citossi, F.; Wallace, M.; Serpell, L. C.; Adams, D. J.; Tovar, J. D. Kinetically Controlled Coassembly of Multichromophoric Peptide Hydrogelators and the Impacts on Energy Transport. *J. Am. Chem. Soc.* **2017**, *139*, 8685–8692.
- (21) Wall, B. D.; Zacca, A. E.; Sanders, A. M.; Wilson, W. L.; Ferguson, A. L.; Tovar, J. D. Supramolecular polymorphism: Tunable electronic interactions within  $\pi$ -conjugated peptide nanostructures dictated by primary amino acid sequence. *Langmuir* **2014**, *30*, 5946–5956.
- (22) Squires, T. M.; Mason, T. G. Fluid Mechanics of Microrheology. *Annu. Rev. Fluid Mech.* **2010**, *42*, 413–438.
- (23) Larsen, T. H.; Furst, E. M. Microrheology of the liquid-solid transition during gelation. *Phys. Rev. Lett.* **2008**, *100*, 1–4.
- (24) Adolf, D.; Martin, J. E. Time-cure superposition during crosslinking. *Macromolecules* **1990**, *23*, 3700–3704.
- (25) Larsen, T. H.; Branco, M. C.; Rajagopal, K.; Schneider, J. P.; Furst, E. M. Sequence-Dependent Gelation Kinetics of  $\beta$ -Hairpin Peptide Hydrogels. *Macromolecules* **2009**, *42*, 8443–8450.
- (26) Spano, F. C.; Silva, C. H.- and J-aggregate behavior in polymeric semiconductors. *Annu. Rev. Phys. Chem.* **2014**, *65*, 477–500.
- (27) Kelly, S. M.; Jess, T. J.; Price, N. C. How to study proteins by circular dichroism. *Biochim. Biophys. Acta, Proteins Proteomics* **2005**, *1751*, 119–139.
- (28) Locklin, J.; Youk, J. H.; Xia, C.; Park, M. K.; Fan, X.; Advincula, R. C. Nanostructured ultrathin films of water-soluble sexithiophene bolaform amphiphiles prepared by layer-by-layer self-assembly. *Langmuir* **2002**, *18*, 877–883.
- (29) Mansbach, R. A.; Ferguson, A. L. Control of the hierarchical assembly of  $\pi$ -conjugated optoelectronic peptides by pH and flow. *Org. Biomol. Chem.* **2017**, *15*, 5484.
- (30) Brunsved, L.; Folmer, B. J. B.; Meijer, E. W.; Sijbesma, R. P. Superamolecular Polymers. *Chem. Rev.* **2001**, *101*, 4071–4098.
- (31) Mason, T. G.; Ganesan, K.; van Zanten, J.; Wirtz, D.; Kuo, S. Particle Tracking Microrheology of Complex Fluids. *Phys. Rev. Lett.* **1997**, *79*, 3282–3285.
- (32) Mason, T. G. Estimating the viscoelastic moduli of complex fluids using the generalized Stokes-Einstein equation. *Rheol. Acta* **2000**, *39*, 371–378.
- (33) Bird, R. B.; Armstrong, R. C.; Hassager, O. *Dynamics of Polymeric Liquids, Vol. 1: Fluid Mechanics*, 2nd ed.; John Wiley & Sons: York, Canada, 1987.
- (34) Winter, H. H.; Chambon, F. Analysis of Linear Viscoelasticity of a Crosslinking Polymer at the Gel Point. *J. Rheol.* **1986**, *30*, 367.
- (35) Chambon, F.; Winter, H. H. Linear Viscoelasticity at the Gel Point of a Crosslinking PDMS with Imbalanced Stoichiometry. *J. Rheol.* **1987**, *31*, 683.
- (36) Valentine, M. T.; Kaplan, P. D.; Thota, D.; Crocker, J. C.; Gisler, T.; Prud'homme, R. K.; Beck, M.; Weitz, D. A. Investigating the microenvironments of inhomogeneous soft materials with multiple particle tracking. *Phys. Rev. E: Stat. Phys., Plasmas, Fluids, Relat. Interdiscip. Top.* **2001**, *64*, 061506.
- (37) Würthner, F. Perylene bisimide dyes as versatile building blocks for functional supramolecular architectures. *Chem. Commun. (Cambridge, U. K.)* **2004**, *1564–1579*.
- (38) Jiménez, Á J.; Lin, M.-J.; Burschka, C.; Becker, J.; Settels, V.; Engels, B.; Würthner, F. Structure-property relationships for 1,7-diphenoxyl-perylene bisimides in solution and in the solid state. *Chemical Science* **2014**, *5*, 608.
- (39) Sanders, A. M.; Dawidczyk, T. J.; Katz, H. E.; Tovar, J. D. Peptide-Based Supramolecular Semiconductor Nanomaterials via Pd-Catalyzed Solid-Phase “Dimerizations”. *ACS Macro Lett.* **2012**, *1*, 1326–1329.
- (40) Vadehra, G. S.; Wall, B. D.; Diegelmann, S. R.; Tovar, J. D. On-resin dimerization incorporates a diverse array of  $\pi$ -conjugated functionality within aqueous self-assembling peptide backbones. *Chem. Commun. (Cambridge, U. K.)* **2010**, *46*, 3947–3949.
- (41) Crocker, J.; Grier, D. Methods of Digital Video Microscopy for Colloidal Studies. *J. Colloid Interface Sci.* **1996**, *179*, 298–310.
- (42) Chen, K.; Anthony, S. M.; Granick, S. Extending particle tracking capability with Delaunay triangulation. *Langmuir* **2014**, *30*, 4760–4766.
- (43) Savin, T.; Doyle, P. S. Static and dynamic errors in particle tracking microrheology. *Biophys. J.* **2005**, *88*, 623–638.
- (44) Rich, J. P.; McKinley, G. H.; Doyle, P. S. Size dependence of microprobe dynamics during gelation of a discotic colloidal clay. *J. Rheol.* **2011**, *55*, 273.
- (45) Valentine, M.; Perlman, Z.; Gardel, M.; Shin, J.; Matsudaira, P.; Mitchison, T.; Weitz, D. Colloid Surface Chemistry Critically Affects Multiple Particle Tracking Measurements of Biomaterials. *Biophys. J.* **2004**, *86*, 4004–4014.